Advances in full-flow penetrometer testing

C. D. O'Loughlin
Centre for Offshore Foundation Systems, University of Western Australia, Perth, Australia,
conleth.oloughlin@uwa.edu.au

D.J. White
University of Southampton, Southampton, UK, david.white@soton.ac.uk

M.F. Randolph[1], Z. Zhou[2]
Centre for Offshore Foundation Systems, University of Western Australia, Perth, Australia,
mark.randolph@uwa.edu.au[1], zefeng.zhou@uwa.edu.au[2]

S.A. Stanier
University of Cambridge, Cambridge, UK, sas229@cam.ac.uk

ABSTRACT: The benefits of full-flow (T-bar and ball) penetrometers in determining both intact and remoulded strengths in soft soils are well recognised. A recently developed numerical solution for interpreting dissipation of excess pore pressure around a ball penetrometer has allowed for the added benefit of measuring consolidation coefficient using a ball penetrometer equipped with pore pressure sensors (termed a 'piezoball') to be realised. Application of the new piezoball solution and the well-established Teh and Houlsby piezocone solution to centrifuge and field data shows that the back-figured consolidation coefficients for both penetrometers are essentially identical. However, an important observation is that for practically-sized penetrometers, dissipation is faster for the spherical geometry of the piezoball than for the conical geometry of the piezocone, allowing time and cost savings to be realised.

Recommendations for real time data processing of penetrometer data are provided. These relate to quantifying the drainage response using a combination of indicators measured during penetration, and 'on-the-fly' calculation of the coefficient of consolidation following episodes of pore pressure dissipation. These data can be used to assess (on site) whether the strength derived from the penetrometer test is undrained or partially drained, or is enhanced due to strain rate effects. These data, combined with advances in actuation control allow an appropriate penetration velocity for certain stages of the penetrometer test to be selected such that the measurements relate to a 'true' (and minimum, i.e. non-rate enhanced) undrained strength.

Additional test protocols are introduced that involve episodes of cyclic loading with intervening consolidation periods. The cycles may involve either large amplitude cyclic displacements or small-amplitude load cycling to provide the remoulded soil strength and a 'cyclic strength' respectively. Such tests provide a means of quantifying the changes in strength that accompany episodes of cyclic remoulding/loading and reconsolidation, which when interpreted within a critical state based effective stress framework provide parameters that may be used in design. The paper provides example data using such test protocols that show significant increases in the strength of soft normally or lightly-overconsoildated soils from reconsolidation. These consolidation-induced gains in strength can almost surpass the reduction in strength due to remoulding, and can more than double the initial soil strength after phases of one-way cyclic loading. These changes in strength have practical relevance to many types of cyclically-loaded offshore infrastructure. 'Smart' penetrometer tests using these new protocols provide a basis to calibrate the relevant soil behaviour for design purposes.

Keywords: T-bar and piezoball penetrometers; cyclic loading; remoulding; consolidation; offshore design

1. Introduction

Full-flow penetrometers, such as the T-bar and piezoball (see Figure 1), were initially developed for research use in the geotechnical centrifuge for strength characterisation (Stewart and Randolph, 1991). They have now been widely adopted in engineering practice offshore (e.g. Kelleher and Randolph 2005; Borel et al. 2005; Peuchen et al. 2005; Kelleher et al. 2010; Borel et al. 2010). Full-flow penetrometers are attractive offshore as reliable intact and remoulded strength characteristics can be determined with a single tool, with consolidation characteristics also available from full-flow tools equipped with pore pressure sensors (Low et al. 2007; DeJong et al. 2008; Colreavy et al. 2016a, 2016b). Minimising testing time is a particular driver for offshore SI as geotechnical SI vessels may cost in the region of $0.25M/day to have on site.

The ability to determine accurate strength profiles without the delay associated with sample recovery to an onshore laboratory is attractive. Full-flow penetrometers also offer benefits in not requiring a correction for overburden, unlike the cone penetrometer, since the full flow mechanism leads to stress equivalence above and below the tool (neglecting the small cross sectional area of the shaft relative to the projected area of the tool). Conversion factors for transforming full-flow penetrometer resistance to soil strength have rigorous theoretical solutions, with relatively minor influence of other soil properties such as rate-dependency and strain-softening behaviour, in contrast to the cone penetrometer for which the resistance is also affected by the soil stiffness and in-situ stress ratio (K_0).

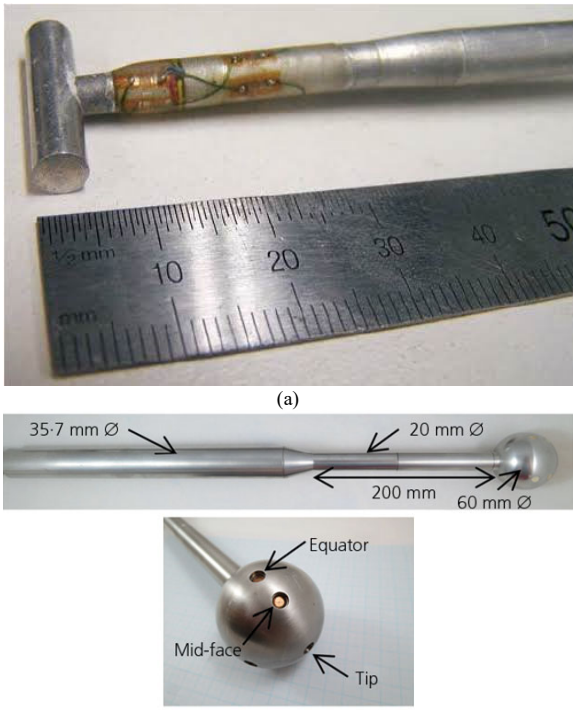

(a)

(b)

Figure 1. Full-flow penetrometers: (a) T-bar (centrifuge scale); (b) piezoball (field scale).

It is recommended that full-flow penetrometer tests include episodes of cyclic remoulding, allowing the degradation of strength from the intact to the fully remoulded value to be quantified, and also as a check on load cell offsets (Randolph et al. 2007).

The ball penetrometer is particularly suited for offshore use as (unlike the T-bar) the axisymmetry avoids load cell bending and the geometry is suited to downhole testing. Pore pressure sensors have recently been added to the ball penetrometer, leading to the term 'piezoball' (Peuchen et al., 2005; Low et al., 2007; Boylan et al., 2007; DeJong et al., 2008; Colreavy et al., 2016a, 2016b), allowing consolidation characteristics to be assessed during a pause in the penetration where the pore pressure is monitored during dissipation, similar to dissipation phases in a cone penetrometer test.

One purpose of determining the consolidation coefficient is to estimate the duration over which changes in soil strength due to drainage will occur. A logical extension is to adopt test protocols that combine episodes of disturbance and dissipation, to allow the changes in strength to be quantified in addition to the rate of dissipation. The 'disturbance' may be large amplitude cycles that fully remould the soil and involve actuating the penetrometer in displacement control, or alternatively low amplitude 'pre-failure' cycles that involve much lower displacements with the actuation conducted in load control.

Both modes are relevant to different design scenarios, particularly offshore. Cyclic loading as a pipe is laid on the seabed causes a loss of strength due to remoulding, but the consolidation process leads to higher friction in the long term (White et al. 2017). Further changes in strength occur as a result of sliding failure beneath pipelines and foundations during in-service thermal expansion and contraction (Cocjin et al. 2017; White et al. 2017). Other offshore cyclic loading scenarios are also less severe, such as one-way cyclic loading of an anchor (Wong et al. 2012; Zhou et al. 2020b). In this case the cyclic loads do not exceed the monotonic capacity, in contrast to the soil flow during large amplitude cycles of a full-flow penetrometer, which strains the soil beyond failure. The regain in soil strength from this lower-amplitude cycling has received less attention, despite its higher relevance for most offshore design problems.

This paper provides examples of the use of full-flow penetrometers in the following areas (as discussed above):

- measurement of intact and remoulded soil strength,
- measurement of consolidation characteristics, and
- observing and quantifying consolidation-induced changes in soil strength

2. Measurement of intact and undrained shear strength

Example depth profiles of net penetration resistance are provided in Figure 2 from tests in normally consolidated kaolin clay in a geotechnical centrifuge, and in Figure 3 from field tests in Ballina clay (New South Wales, Australia). Both testing campaigns employed T-bar, piezoball and piezocone testing.

Further details on these centrifuge and field tests are provided in Colreavy et al. (2016a) and Colreavy et al. (2016b) respectively. The net penetration resistance profiles for the three penetrometers are broadly similar, which implies that, for these soils, a similar T-bar, ball and cone factor would be appropriate to deduce the undrained shear strength.

It is worth noting that the piezocone resistance required correction for temperature effects. The basis of this correction was to adjust the output from the load cell strain gauges to account for changes in temperature relative to the soil surface. The effect of change on temperature on the piezocone load cell strain gauge output was assessed in the laboratory prior to the field tests (Suzuki 2015). A correction was then applied to the measured penetration test based on the measured profile of temperature with penetration depth. Applying this correction to the piezocone resistance resulted in a reduction of the measured resistance by up to 50%. Although the T-bar tests were carried out with the same piezocone penetrometer (replacing the conical probe with the T-bar), the larger projected area resulted in minimal correction to the T-bar penetration resistance (< 3%). Similarly, the temperature effect on the piezoball penetration resistance was negligible.

The excess pore pressure developed by the passage of the penetrometers is also shown in Figures 2 and 3. The excess pore pressures generated around the piezoball reflect the stress distribution (Boylan et al. 2010). The field scale piezoball measured pore pressure at the tip, mid-face and equator position, whereas measurements on the centrifuge scale piezoball were limited to the mid-face and equator positions due to space constraints on the much smaller device. At the tip, where compressive

stresses are high, excess pore pressures are expected to be high. At the equator position, the soil is primarily subjected to pure shear, which will generate either positive or negative excess pore pressure depending on whether the soil exhibits contractive or dilative behaviour. At the mid-face position, the stresses are a combination of compression and shear, such that the magnitude of the excess pore pressure should lie between those at the tip and equator. This is confirmed by Figure 3, which compares excess pore pressures generated around the piezoball and piezocone in the field tests. The excess pore pressure measured by the piezocone at the u_2 position is closest to (but lower than) the excess pore pressure at the piezoball mid-face position, similar to the centrifuge measurements on Figure 2, although between 0 and 6 m (in the field) Δu_2 is much lower.

Figure 2 also shows sharp reductions in excess pore pressure at discrete depths. These correspond to the depths where dissipation tests were conducted for both the piezocone and the piezoball, as considered later in the paper. The increase in penetration resistance immediately beneath these depths reflects the consolidation-induced strength changes that occur in the soil locally around the penetrometer probe, and provides a hint to other test protocols that can be adopted to quantify this response, as described later in the paper.

Figure 4 shows the reduction in penetration resistance during repeated cycles of moving the penetrometer vertically about a discrete depth. In both the centrifuge and the field tests a near-steady resistance is mobilised after about five cycles, with the ratio of the initial (intact) resistance to the eventual resistance providing an indication of the sensitivity of the soil. The sensitivity measurement from the centrifuge tests is $S_t = 2.5$, which is consistent with the (remoulded) soil strength mobilised in continuous penetration problems, e.g. suction caisson installation (Andersen et al. 2005) or in pipeline installation (White et al. 2015). The cyclic phase of the field penetrometer tests suggests a sensitivity in the range $S_t = 2.6$ to 3.2, which is much more consistent than equivalent estimates from field shear vane tests which are in the range $S_t = 1.3$ to 5.6.

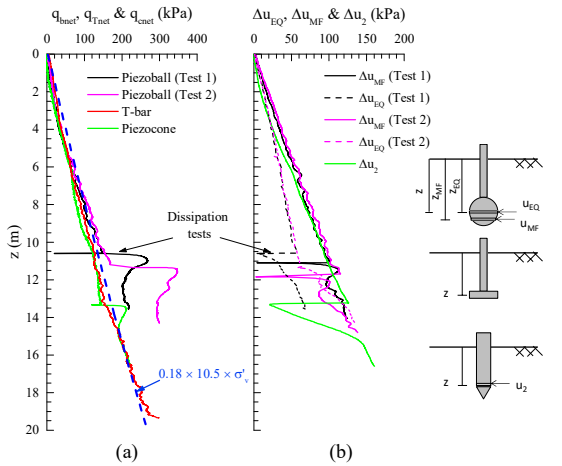

Figure 2. Penetration profiles from centrifuge tests in normally consolidated kaolin clay: (a) net penetration resistance for piezoball, T-bar and piezocone; (b) excess pore pressure for piezoball mid-face and equator and piezocone u_2 measurement locations.

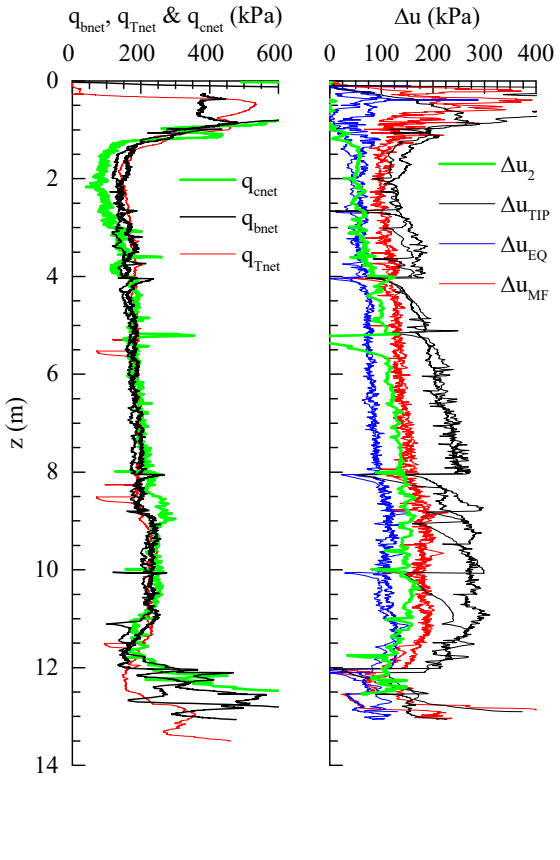

Figure 3. Penetration profiles from field tests in Ballina clay: (a) net penetration resistance for piezoball, T-bar and piezocone; (b) excess pore pressure for piezoball tip, mid-face and equator and piezocone u_2 measurement locations.

It is worth noting that the field test profiles in Figure 3 adopted the recommended penetration velocity, v = 20 mm/s (Lunne et al., 1997), whereas the penetration velocity in the centrifuge test was between v = 0.56 mm/s and v = 1.13 mm/s to ensure that the dimensionless velocity, $V' = vD_e/c_h = 30$ (where D_e is defined as the diameter of a circle with the same projected area of the penetrometer probe and c_h is the coefficient of horizontal (rather than vertical) consolidation) was the same for each penetrometer and sufficient to generate a primarily undrained response (House et al. 2001; Randolph and Hope, 2004).

Targeting an undrained response in the centrifuge tests was possible as c_h is well established for this soil and known ahead of the test. This becomes more difficult in a field test where little or no knowledge of c_h may be available beforehand. Hence, care is required to ensure that the response in the field test is indeed undrained, if the penetration response is to be interpreted to an undrained strength or used to trigger a dissipation test. This is made evident in Figure 5, which shows the change in net penetration resistance as the penetration velocity was reduced (in a 'twitch' test, House et al. 2001) over three orders of magnitude, from v = 20 mm/s to v = 0.02 mm/s. The data are presented as net penetration resistance normalised by the net penetration resistance at v = 20 mm/s,

$q_{bnet}/q_{bnet(ref)}$, against the non-dimensional velocity, V', using c_h estimated from the piezoball mid-face dissipation tests, following penetration at 20 mm/s (described later in the paper). An important observation from Figure 5 is that the standard penetration velocity, v = 20 mm/s, is over two orders of magnitude higher than the penetration velocity that results in undrained conditions. This results in a net penetration resistance, and hence a derived undrained shear strength that is approximately 40% higher than the minimum (arguably the most appropriate design undrained) value. The observations made here are for a piezoball penetrometer, but will also apply to other penetrometers including the piezocone, provided that the strain rates, which may be approximated by v/D, are similar.

Conversely, using the same standard penetration velocity in a silt with c_h = 10,000 m^2/year results in V' = ~2 for a 35 .7 mm diameter piezocone and V' = ~4 for a 60 mm diameter piezoball, sufficiently low to generate partially drained conditions. This was demonstrated by Erbich (2005), summarised here in Figure 6, who showed that in the sandy silts at the Yolla field, with a typical c_v = 7000 m^2/year, T-bar and cone penetrometer tests (CPTs) performed at a penetration velocity of 20 mm/s result in V = 3.9 and 3.6 for the CPT and T-bar respectively.

These tests are likely to have been affected by partial drainage during penetration. If a strength had been interpreted from the results using a standard undrained bearing factor, N_{kt}, the deduced strength would have been higher than the undrained strength that would be mobilised by a much larger foundation – in this case an 18.2 m diameter spudcan penetrating at v ≈ 5.5 × 10^{-4} m/s, such that V = 45.

These two examples show that it is important to assess the likely drainage condition during a penetrometer test in order to assess whether the conventional interpretation to derive undrained strength is appropriate or not, and to assess the level of viscous rate enhancement. This aspect of CPT interpretation has been recognised (e.g. Erbrich 2005) but is not always considered in practice. In the next section of this paper, we explore methods to assess the consolidation coefficient, which assists in identification of partial drainage or viscous enhancement of penetrometer resistance, based on existing data provided by conventional penetrometer tests, and novel approaches.

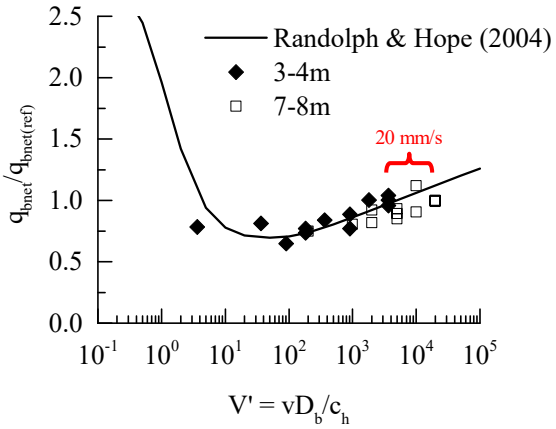

Figure 5. Piezoball backbone curves of net penetration resistance

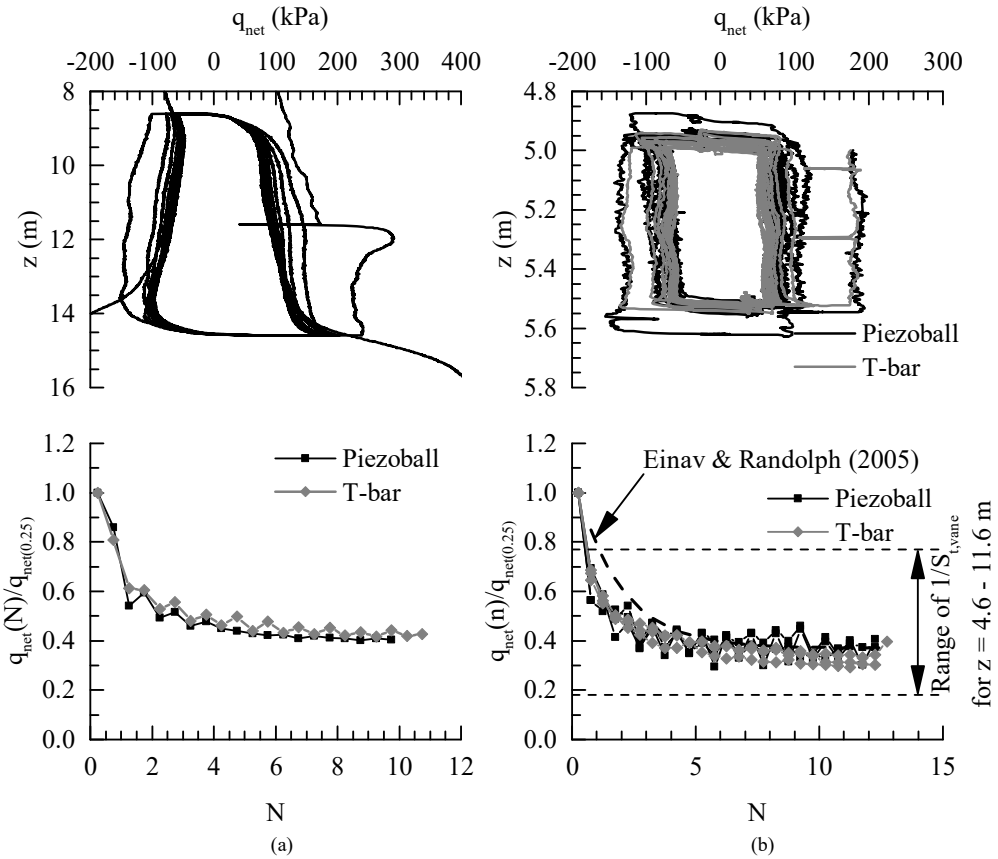

Figure 4. Piezoball and T-bar cyclic remoulding response: (a) centrifuge tests in kaolin clay; (b) field tests in Ballina clay.

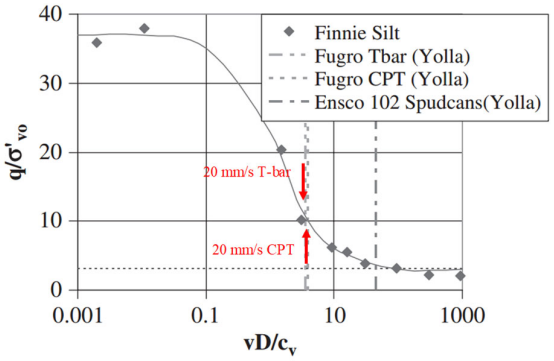

Figure 6. Partial drainage during T-bar and CPT tests at Yolla (after Erbrich, 2005).

3. *Quantifying the coefficient of consolidation from piezoball dissipation data*

Quantifying the coefficient of consolidation from dissipation data involves matching the measured response with a theoretical or numerical solution. In the case of a piezocone, the solution adopted is typically that provided by Teh and Houlsby (1991). An equivalent solution (Mahmoodzadeh et al. 2015) has recently been developed for the piezoball – based on large deformation finite element analyses – offering an opportunity to measure intact and remoulded strength, and also the coefficient of consolidation in a single penetrometer test. The validity of the new piezoball solution has been checked by making comparisons with centrifuge and field data as described in Mahmoodzadeh et al. (2015) and Colreavy et al. (2016a, 2016b); brief details are summarised here.

3.1. *Experimental dissipation responses*

Experimental dissipation responses from the centrifuge and field tests considered earlier are shown in Figure 7 together with corresponding piezocone dissipation curves conducted at the same depth. The initial magnitudes of excess pore pressure, Δu_2, Δu_{MF} and Δu_{EQ} reflect the pore pressure generated during penetration. Similar values are recorded at the piezocone u_2 location and the piezoball mid-face location, whereas the piezoball equator excess pore pressure is 57 - 64% of the u_2 and mid-face values.

The centrifuge and field examples both show immediate decay of Δu_{MF}, whereas Δu_2 and Δu_{EQ} both show an initial rise with dissipation time, t. In the centrifuge tests the rise amounts to no greater than 6% of the initial value and occurs over less than 10 seconds, whereas in the field tests the rise in pore pressure relative to the initial value is higher, at 22% for Δu_2 and 18% for Δu_{EQ}, occurring over 20 seconds. This response is commonly observed. Although it has often been attributed to poor filter saturation, it is now considered to reflect redistribution of pore pressures from the face to the shoulder of the cone and around the circumference of the ball (Chai et al. 2012; Mahmoodzadeh et al. 2015).

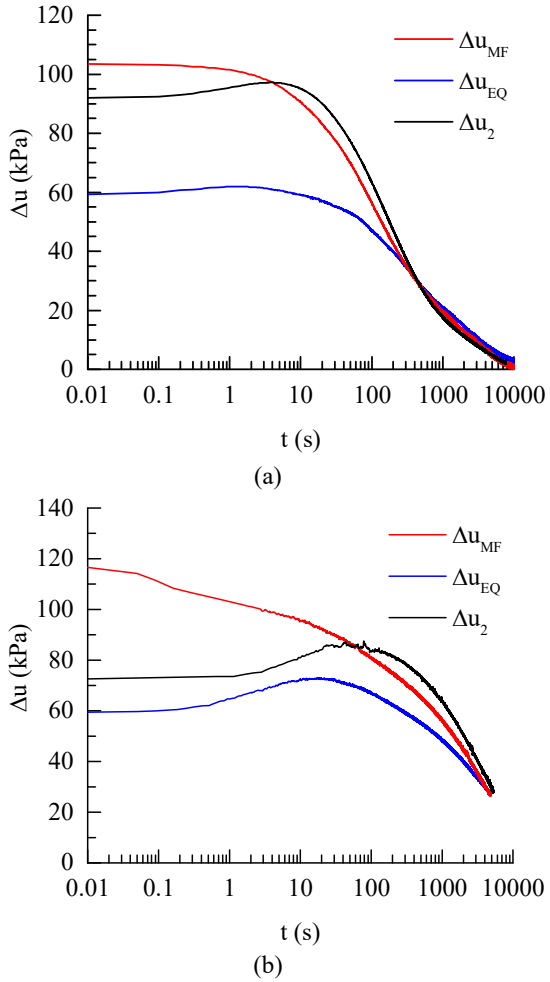

Figure 7. Centrifuge and field piezoball and piezocone dissipation–time responses: (a) kaolin clay, (b) Ballina clay.

In absolute measures of time (i.e. for the actual cone and ball probe diameters, accepting that these values will affect the relative consolidation durations), excess pore pressures dissipate to 50% of their initial value more quickly for the piezoball at the u_{MF} location than for the piezocone at the u_2 location. This observation is interesting as the diameter of the piezoball is twice that of the piezocone and hence drainage path lengths are expected to be longer. However, the response is accelerated by the three-dimensionality of the flow, and the opportunity for high mid-face pore pressures below the equator to equalise against lower mid-face pore pressures above the equator – which occurs over a very short drainage distance.

This point is illustrated by Figure 8, which plots the normalised excess pore pressure response, $U = \Delta u/\Delta u_i$, against a common form of non-dimensional time, $T^* = c_h t/D^2 I_r^{0.5}$ for both devices, where the rigidity index, $I_r = 88$ for the kaolin clay and $I_r = 80$ for the Ballina clay. The initial excess pore pressure, Δu_i, was estimated at $\sqrt{t} = 0$ using the extrapolation method described by Sully et al. (1999). This method accounts for redistribution of pore pressure around the ball before dissipation, although in several instances Δu_i calculated using this approach gave very similar values to the measured value at t = 0. In passing it should be noted that Mahmoodzadeh et al. (2015) showed that for the piezoball the most appropriate

time normalisation is $T_b = c_h t/D_b d_s I_r^{0.25}$, where D_b and d_s are the diameters of ball and shaft respectively.

Figure 8 shows that excess pore pressures dissipate more efficiently around the piezoball than around the piezocone, as both the piezoball mid-face and equator non-dimensional times for U = 0.5 are much lower than for the piezocone. The non-dimensional time for 50% excess pore pressure dissipation, T_{50}^*, for the equator is 67% of the piezocone value while T_{50}^* for the mid-face is 22% of that for the piezocone – about five times faster.

For the mid-face, this reduction in T_{50} more than compensates for the larger diameter of the ball compared with the piezocone, so that absolute t_{50} values are also smaller for the piezoball.

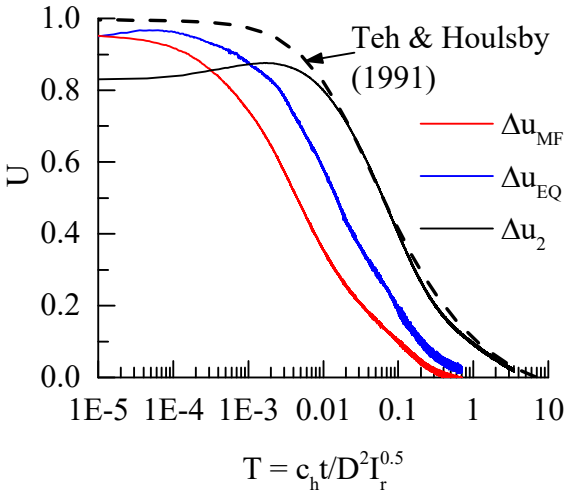

(a)

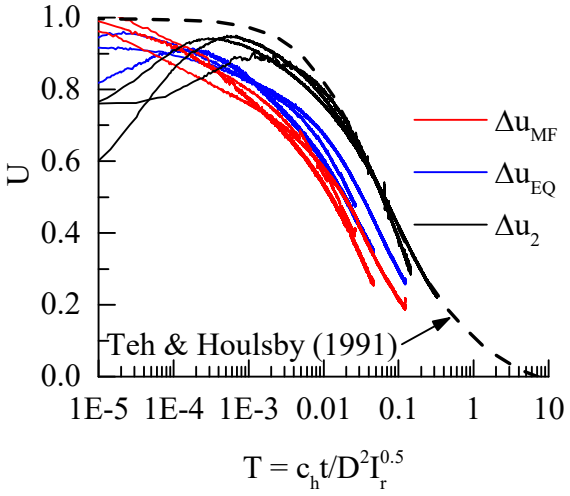

(b)

Figure 8. Centrifuge and field piezoball and piezocone dissipation – non dimensional time responses: (a) kaolin clay, (b) Ballina clay

3.2. Determining c_h from piezocone and piezoball dissipation data

Figure 8 also shows the Teh and Houlsby (1991) theoretical solution for the piezocone. The best match between the experimental dissipation data and the Teh and Houlsby solution was obtained using c_h = 0.42 mm^2/s for kaolin clay and c_h = 0.31 and 0.08 mm^2/s for Ballina clay at 4 and 8 m depth respectively. Equivalent dissipation data for the piezoball are plotted on Figure 9 and Figure 10 for the centrifuge and field data respectively, together with the numerical solution. Better overall agreement between the experimental piezoball data and the numerical solution is observed for the mid-face position than for the equator position. Using the piezoball mid-face dissipation data, the best agreement with the numerical solutions was achieved using c_h = 0.46 mm^2/s for kaolin clay and c_h = 0.33 and 0.06 mm^2/s for Ballina clay at 4 and 8 m depth respectively. These values are essentially identical to those derived from the piezocone, but required 63-65% of the dissipation time to reach t_{50}.

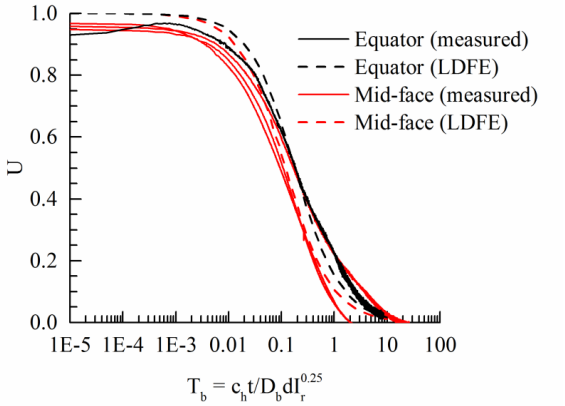

Figure 9. Piezoball dissipation response in kaolin clay compared with the numerical (LDFE) solution

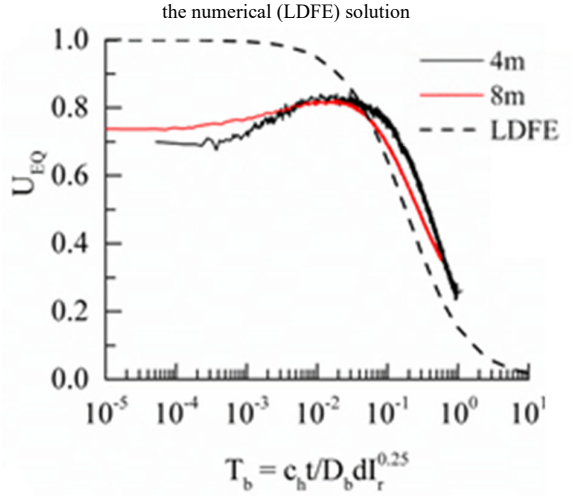

(a)

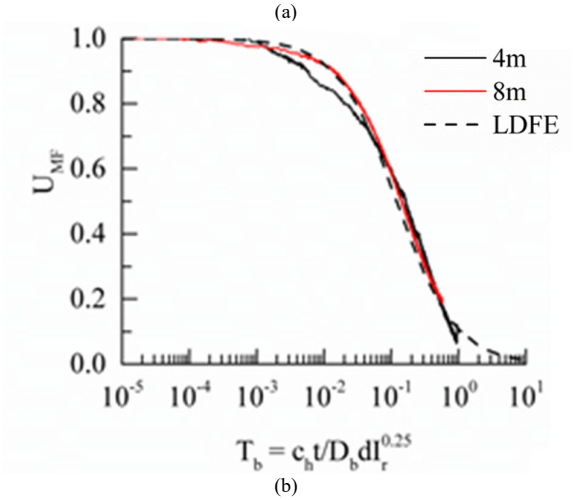

(b)

Figure 10. Comparison between Ballina field piezoball dissipation responses and the theoretical solution: (a) equator, (b) mid-face.

The reduced dissipation time for the piezoball relative to the piezocone can be quantified by considering the time factor, T^*_{50} and T_{b50} at U = 0.5 for either case. The ratio of the absolute times for U = 0.5 can then be written as

$$\frac{t_{b50}}{t_{c50}} = \frac{T_{b50}}{T^*_{50}} \frac{D_b{}^2 \sqrt{A_s/A_b}}{D_c{}^2} \frac{1}{I_r{}^{0.25}} \quad (1)$$

where T^*_{50} = 0.06 and T_{b50} = 0.12 for the piezocone u_2 position and piezoball mid-face position respectively. Examples of dissipation times are provided in Table 1 for a practical range of c_h and I_r values. These assume a typically-sized 60 mm diameter piezoball, i.e. D_b = 60 mm with a shaft to ball area ratio, A_s/A_b = 0.1, and the industry standard 10 cm^2 cone, i.e. D_c = 35.7 mm. Taking as an example, I_r = 100 and c_h = 1 m^2/year, the time for 50% dissipation of the piezocone is 4.6 hours, compared with 2¾ hours for the piezoball, a reduction by a factor of 1.7.

This comparison also highlights the lower dependency on rigidity ratio of the piezoball dissipation, compared to the piezocone. The numerical studies have shown that while the piezocone dissipation time scales with $I_r{}^{0.5}$, the piezoball scales by $I_r{}^{0.25}$. Given that I_r must usually be estimated when interpreting field data, this lower dependency on I_r reduces the resulting uncertainty in c_h from piezoball results compared to piezocone data.

Table 1. Dissipations times for a 10 cm^2 piezocone and a 60 mm diameter piezoball

I_r	Time for 50% dissipation (mins)	c_h (m^2/year)		
		0.1	1	10
10	Piezocone u_2	1236	124	12
	Piezoball mid-face	1302	130	13
100	Piezocone u_2	2763	276	28
	Piezoball mid-face	1947	195	19
1000	Piezocone u_2	3908	391	39
	Piezoball mid-face	2315	232	23

3.3. Assessing drainage condition from on-the-fly penetrometer measurements

As shown by Figures 5 and 6, penetrometer resistance will be affected by the penetration velocity, the penetrometer diameter and the coefficient of consolidation. In addition to the effect on penetration resistance, a further consequence of conducting penetration tests at the 'wrong' velocity is the effect on the subsequent dissipation response. For instance, Figure 11 shows that the overall agreement shown between Ballina field piezoball dissipation data after a penetration rate of 20 mm/s and the numerical solution is quite poor. However, the match in the overall response improves as the penetration velocity reduces, with the best fit obtained for a penetration rate, v = 0.02 mm/s. This penetration velocity corresponds with V' = 4 (4 m) and 20 (8 m), where strain rate effects are least pronounced and the penetration resistance is lowest (see Figure 5).

In this case penetration at v = 20 mm/s is over two orders of magnitude into the viscous range. It is not clear why the higher penetration rate distorts the shape of the subsequent dissipation response. However, the back-calculated c_h is practically identical for each penetration velocity when T_{b50} is matched to the numerical solution.

This observation suggests a possible indicator that the penetration process is in the viscous range, above the 'true' minimal undrained resistance. The mismatch between theoretical/numerical dissipation solutions in the form of the 'corner cutting' evident in the first part of the dissipation response shown in Figure 11a may provide a warning of the viscous enhancement.

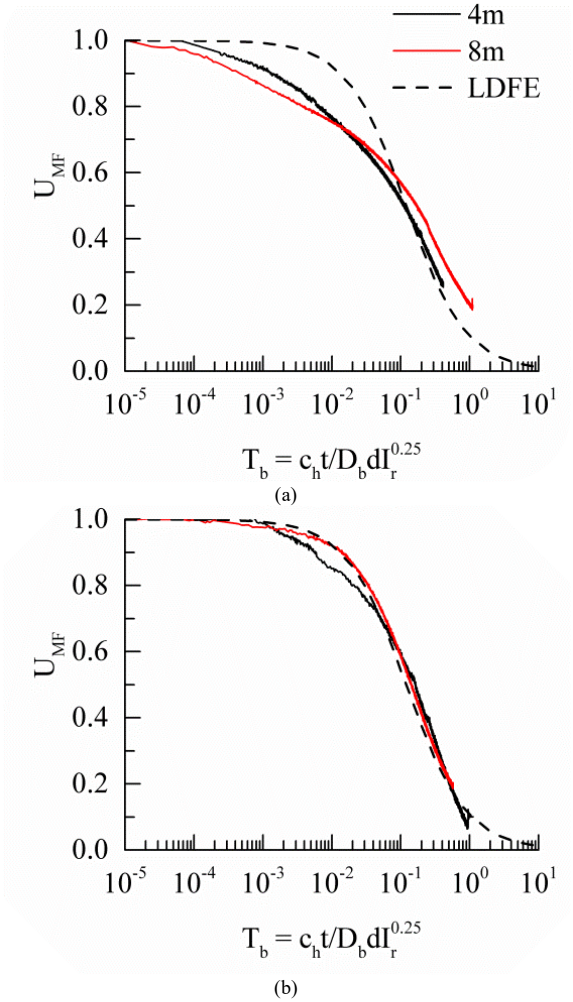

Figure 11. Measured and numerical piezoball excess pore pressure dissipation responses after penetration at: (a) 20 mm/s, (b) 0.02 mm/s.

In contrast, penetration velocities that lead to partially drained conditions result in discrepancies in the back-calculated c_h compared to a dissipation after undrained penetration. This is made clear by Figure 12, which shows dissipation responses from centrifuge piezoball tests in kaolin clay, where dissipation of excess pore pressure was allowed after penetration at velocities, v = 0.056, 0.0056 and 0.002 mm/s (V' = 0.26, 2.56 and 25.6 respectively). Figure 12 shows the mid-face dissipation profiles, where the time-factor, T_b, has been calculated using c_h = 0.3 mm^2/s as established from the match between the dissipation profile following undrained penetration (V' = 25.6) and the numerical (LDFE) solution.

It is evident from Figure 12 that dissipation times increase as the preceding penetration velocity and consequently the initial excess pore pressure reduces. This has consequences for dissipation tests that follow partially drained penetration, as analysis of the dissipation data will result in erroneous estimates of c_h. For example, if the initial penetration was conducted at V' = 0.26, and the subsequent dissipation data were matched with the LDFE solution, the resulting c_h would be approximately 6.5 times lower than that obtained for a dissipation following undrained penetration (V' = 25.6).

Backbone curves such as that (partially) shown by Figure 5 may be used to check the drainage conditions generated during a penetrometer test. This requires knowledge of the coefficient of consolidation, which may be deduced from the dissipation phase of the same test. However, a word of caution is warranted, as a partially drained response will result in a higher calculated V' if c_h is derived from the dissipation following the partially drained penetration. Taking the preceding example where the penetration corresponded to V' = 0.26, a dissipation test to deduce c_h and check the drainage response would result in a calculated V' = 1.7. Although this value still does not indicate an undrained response, the actual V' is still one order of magnitude lower, such that the real drainage effects are masked.

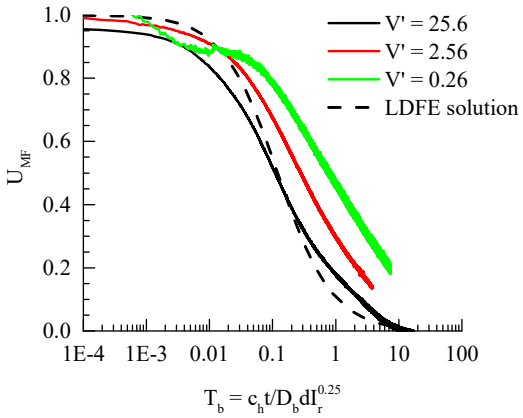

Figure 12. Non-dimensional piezoball dissipation profiles for the piezoball mid-face measurement location following undrained and partially drained penetration.

In summary, the effects from a piezoball or piezocone test being performance at a velocity which is not at the minimum resistance point at the transition between partial drainage and viscous enhancement are:

- higher penetration resistance and hence a higher deduced soil strength, if the effect of partial drainage or viscous enhancement is not recognised and accounted for in the adopted bearing factor, N_{kt} or N_{ball}
- lower confidence in establishing c_h from dissipation data should the penetration velocity lead to conditions that are on the 'viscous' side of undrained behaviour, due to the 'corner cutting' of the dissipation curve relative to theory (this shape of response offers a marker to detect the viscous enhancement),
- erroneous values of c_h established from dissipation data should the penetration velocity lead to conditions that are partially drained.

Given these consequences, it would be beneficial to adopt strategies that would give information on the drainage and viscous response during penetration, such that decisions could be made to adjust the test penetration rate, or to repeat the test under different conditions.

Such strategies may include:

- Observing the pore pressure parameter, B_{ball} or B_q during penetration. As shown by Figure 13 from a combination of centrifuge and field tests, for normally or lightly over consolidated clays, partially drained conditions will occur at $B_{ball} < 0.9$ and 0.6 (for the mid-face and equator positions respectively). However, more data that would improve the definition of these dependencies would improve confidence in these indicative limits for undrained penetration.
- Automated calculation of c_h during a dissipation test. This would allow V' to be calculated during the test, such that an assessment of the influence of either partial drainage or viscous strain rate effects could be made. This strategy would need to be adopted together with monitoring B_{ball} above, as the deduced c_h will already be erroneous if the response is partially drained in a way that masks the influence of partial drainage (as discussed above).

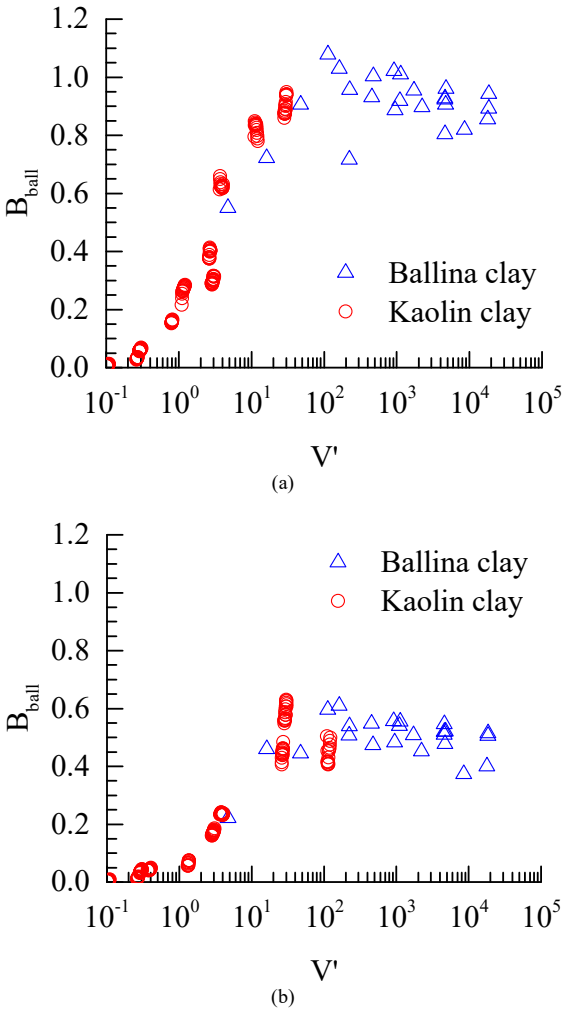

Figure 13. B_{ball} as a partial consolidation indicator: (a) mid-face (b) equator.

4. Evaluating changes in strength during cycles of loading and reconsolidation

As shown earlier in the paper, cyclic T-bar or piezoball penetrometer tests allow for measurement of both intact and remoulded soil strengths, with piezoball dissipation tests providing a means of assessing the consolidation characteristics of soil. One purpose of determining the consolidation coefficient is to estimate the duration over which changes in soil strength due to drainage will occur. Such soil strength increases are evident from the restarts after the dissipation phase of the piezoball tests in Figure 2, where the penetration resistance increases locally due to the higher soil strength following consolidation. A logical extension of standard penetrometer tests is to combine episodes of disturbance and dissipation, to allow the changes in strength to be quantified in addition to the rate of dissipation. Such tests require no additional instrumentation or control, but have a longer duration and require the development of appropriate interpretation methodologies.

An episodic cyclic T-bar penetrometer test performed in kaolin clay was reported by Hodder et al. (2009). This test involved episodes of 20 penetration cycles interspersed with a consolidation period. The loss of strength on remoulding is partly due to the generation of positive excess pore pressure. As this dissipates and the effective stress rises back to the geostatic state the soil densifies and the subsequent undrained shear strength is higher. Figure 14 shows the T-bar strength at a particular depth – 2.25 m – during each cycle. After three episodes of remoulding and reconsolidation, the current remoulded strength was double the initial value and close to the original intact strength.

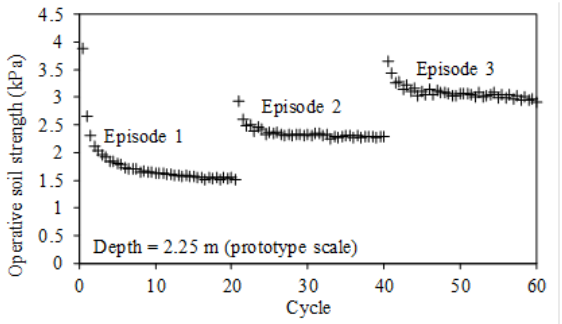

Figure 14. Changes in strength during episodic cyclic T-bar test in kaolin clay (after Hodder et al. 2009).

4.1. Episodic cyclic penetrometer tests

This section presents results from additional centrifuge penetrometer tests in a reconstituted carbonate silt to identify whether penetrometer tests can be extended to quantify changes in soil strength that result from loading and disturbance followed by consolidation. Potential applications include the capacity of foundations, piles and anchors that are subjected to cycles of loading over a period of time during which significant consolidation may occur.

The cyclic sequences were undertaken in either a displacement-controlled mode to simulate large amplitude cyclic loading, or a load-controlled mode to simulate low amplitude (operational) cyclic loading. The displacement-controlled cycles relate to onerous cyclic loading, such as that caused by an oscillating catenary riser pipe where it touches down on the seabed, or by a pipeline as it is laid on the seabed. In such instances the cyclic shear strains are sufficiently high to degrade the soil strength towards the remoulded limit. The load-controlled cycles are more applicable to less severe cyclic loading such as one-way cyclic loading of an anchor, where the cyclic loads do not exceed the monotonic capacity, in contrast to the soil flow during large amplitude cycles which strains the soil beyond failure.

The episodic cyclic T-bar penetrometer tests were conducted in centrifuge samples of a reconstituted carbonate silt at an acceleration level of 150g. Each test involved an initial penetration to at least eight T-bar diameters at a velocity, v = 3 mm/s to ensure that response was primarily undrained ($vD/c_h = 53$). This was followed by episodes of cyclic loading interspersed with pause periods for consolidation. The cyclic phase was conducted either in displacement control by moving the T-bar vertically by ± 4.5 diameters for N = 20 cycles, or in load control between load limits that mobilised either 0% and 75% or 25% and 75% of the intact penetration resistance (and therefore the initial undrained shear strength, $s_{u,i}$) for either N = 20 or 1,080 cycles. A consolidation period of t_c = 1 hour was allowed between each cyclic phase, during which the T-bar was held at the middle of the cyclic zone.

One test involved a single consolidation period after the initial penetration – with no cyclic loading – to quantify the change in strength after consolidation with and without a cyclic loading phase. The testing protocol followed for each test type is shown in Figure 15 and further details on the tests are provided in O'Loughlin et al. (2019).

Example results are provided in Figure 16a and 16b for the displacement- and load-controlled cyclic loading respectively. The significant reduction in soil strength during the large amplitude (displacement-controlled) cycles is evident in Figure 16a, although the limiting remoulded strength increases as more consolidation is permitted, i.e. with increasing number of episodes. In contrast the low amplitude (load-controlled) one-way cycles do not reduce soil strength, with consolidation periods leading to soil strengths that are significantly higher than the intact strength.

The changes in s_u from both the small-amplitude load-controlled cycles and the large-amplitude displacement-controlled cycles are summarised in Figure 17, leading to the following observations:

- The displacement-controlled cycles (Test 8) fully remould the soil causing a significant reduction in strength. In contrast, the load-controlled cycles cause minimal reduction in soil strength (<5%), even though each cycle mobilises $0.75s_{u,i}$.
- The increase in s_u after the consolidation period following each load-controlled cyclic episode is significant, with strengths of $2.0s_{u,i}$ and $2.3s_{u,i}$ reached after the first and second consolidation periods. These post-consolidation strengths are typically 2-3 times greater than observed after the displacement-controlled cycles.

- Consolidation immediately following the initial penetration (i.e. without load cycles; Test 7 in Figure 17) lead to a significant increase in s_u, to ~1.7$s_{u,i}$. However, a greater strength is measured when the consolidation period is preceded by a cyclic episode (Test 9b), which generates additional excess pore pressure.

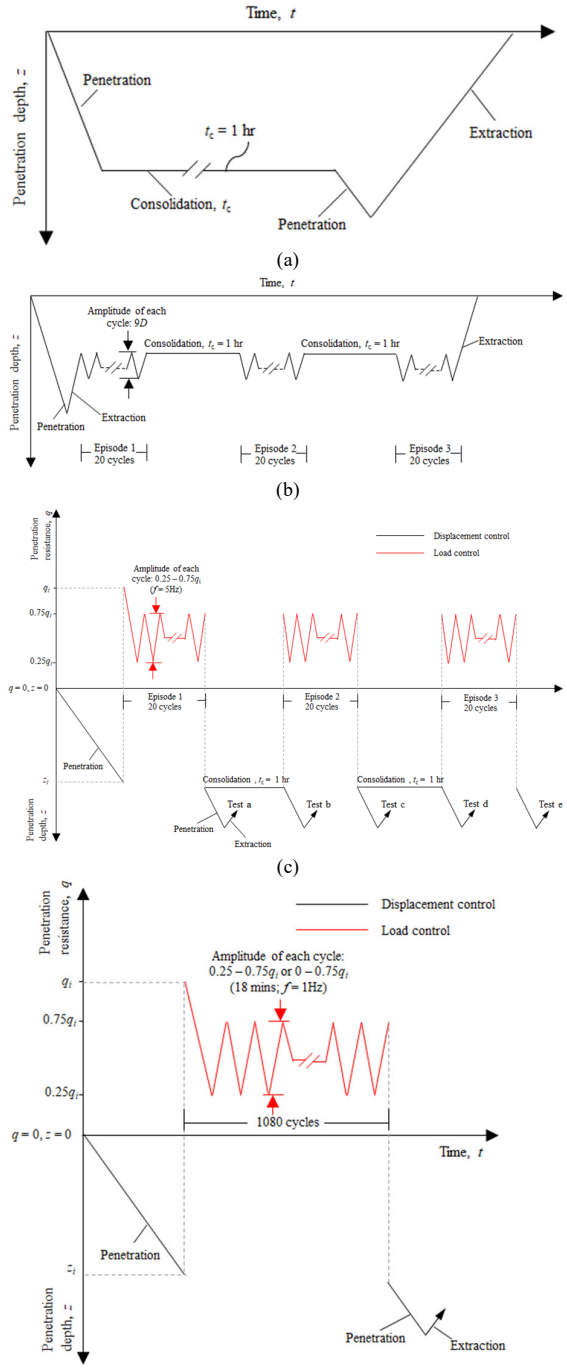

Figure 15. Episodic cyclic penetrometer test procedures: (a) Type I (load-control); (b) Type II (displacement-control); (c) Type III (load-control); (d) Type IV (load-control).

- Continued cyclic loading for N = 1,080 cycles in a single episode (reflecting the number of cycles that might occur in a typical three-hour storm) lead to an increase in s_u by 2.35 times in Test 10 (which cycled from 0.25-0.75q_i), and by 2.9 times in Test 11 (which cycled from 0-0.75q_i). There was no subsequent consolidation period but consolidation would have occurred concurrent with the cycles. These increases are slightly higher than the strength gain from three N = 20 cyclic episodes with intervening t_c = 1 hour consolidation periods.

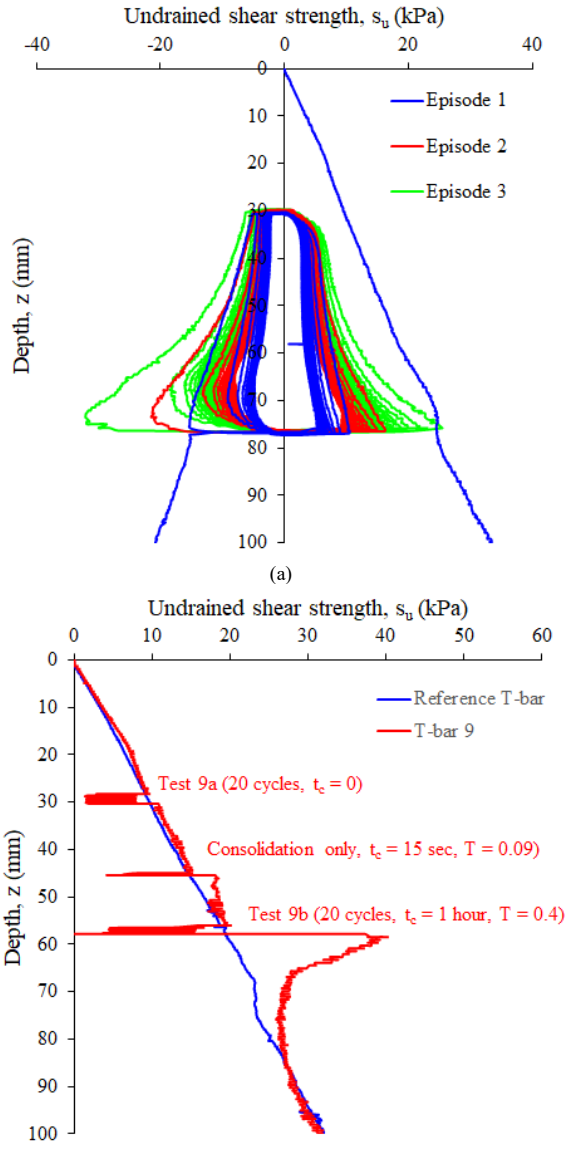

Figure 16. Changes in soil strength from: (a) displacement-controlled cycles (Type II); (b) load-controlled cycles (Type III).

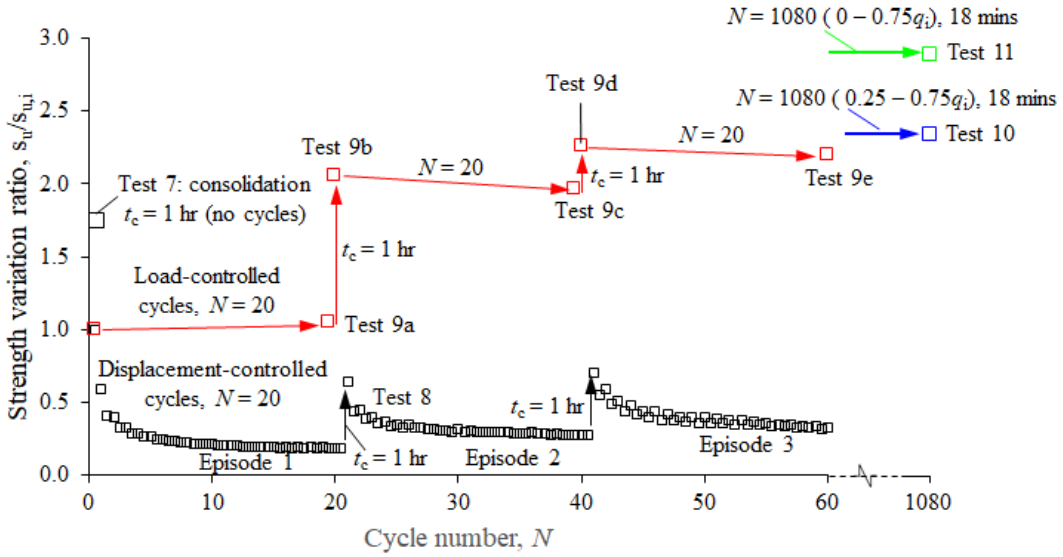

Figure 17. Comparison of changing soil strength due to load and displacement controlled loading cycles in centrifuge penetrometer tests in a reconstituted normally consolidated carbonate silt.

4.2. Potential for practical applications

Episodic tests involving multiple periods of dissipation have a longer duration than conventional penetrometer tests and require the development of appropriate interpretation methodologies.

The required duration of these tests can be estimated from (i) the time allowed for dissipation after each episode and (ii) the requirement for, say, three to five episodes (noting that in the tests reported here, a steady state was still not reached after three episodes). The dissipation period could be the T_{90} period, allowing virtually full dissipation and simplifying the interpretation. Alternatively, only partial dissipation could be allowed, which would yield greater measurable strength gain for a given test duration. This was the case for the tests considered here, where the dissipation period corresponds with $T = 0.4 \approx T_{70}$ (assuming the numerical solution for the piezoball equator position is broadly applicable to the T-bar). Had T_{90} been adopted for the dissipation phases the overall test duration would have been at least three times longer.

Figure 18 shows the variation in overall test durations for three episodes and for both T_{50} and T_{90} dissipations, using the numerical solution for the piezoball (at the equator location) for I_r = 100. The calculated durations on Figure 18 are for three episodes of 20 load- or displacement-controlled cycles with intervening consolidation periods, and cover both model and field scale penetrometers and a wide range of consolidation coefficients. The penetration and extraction velocities for the displacement-controlled cycles were determined such that $V' = vD/c_h = 30$ (for the different penetrometer diameters and consolidation coefficients, but capped at v = 20 mm/s to satisfy typical actuation limits) to ensure that the cyclic phases maximise pore pressure generation (Colreavy et al. 2016). Likewise, the loading frequency for the load-controlled cycles was taken as 1 Hz and 0.08 Hz for the model and field scale penetrometers respectively. The field scale loading frequency was scaled from the 1 Hz frequency adopted in the model scale tests on Figure 16b by the ratio of the penetrometer diameters (model:field) to account for the higher displacement amplitudes expected with the larger field scale device. Higher frequencies at field scale may be achievable as actuation systems used for field testing become more sophisticated.

The two scales of penetrometer shown in Figure 18 cover both box-core-scale and at-seabed applications. Naturally the in-box-core device leads to more rapid drainage and a shorter overall test duration. Although overall test durations for the in-situ applications are likely to be time-prohibitive using current penetrometer concepts, refinements of the test, such as conducting a larger number of continuous cycles without consolidation periods may be a useful strategy. By way of example, the 1,080 load-controlled cycles included in Figure 17 took 18 minutes at 1 Hz, which would translate to approximately 3.5 hours at field scale as each cycle would take 12 times longer.

Tests in box cores (or in tube samples) can be conducted off the critical path of vessel operations, meaning that the time cost is lower. These tests could even be conducted as part of the onshore laboratory testing program, using tube samples. The actuation and motion control can be fully automated, allowing the test to run unattended.

An alternative option to performing the tests in situ could be to devise a penetrometer system that can be deployed and left in place to test while the mother ship performs other operations, reducing the cost associated with a long test duration. Such a device would harness the emergent capabilities offered by remote and autonomous technologies. These ideas, and the new test protocols outlined in this paper, make a step towards a future vision for geotechnical investigation methods. Perhaps future surveys will be performed by autonomous underwater vehicles (AUVs), equipped with intelligent micromachines, carrying tools that probe the seabed in a manner designed to mimic construction and operation. Such systems will give richer measurements that provide more robust estimates of soil parameters that are more directly applicable in design.

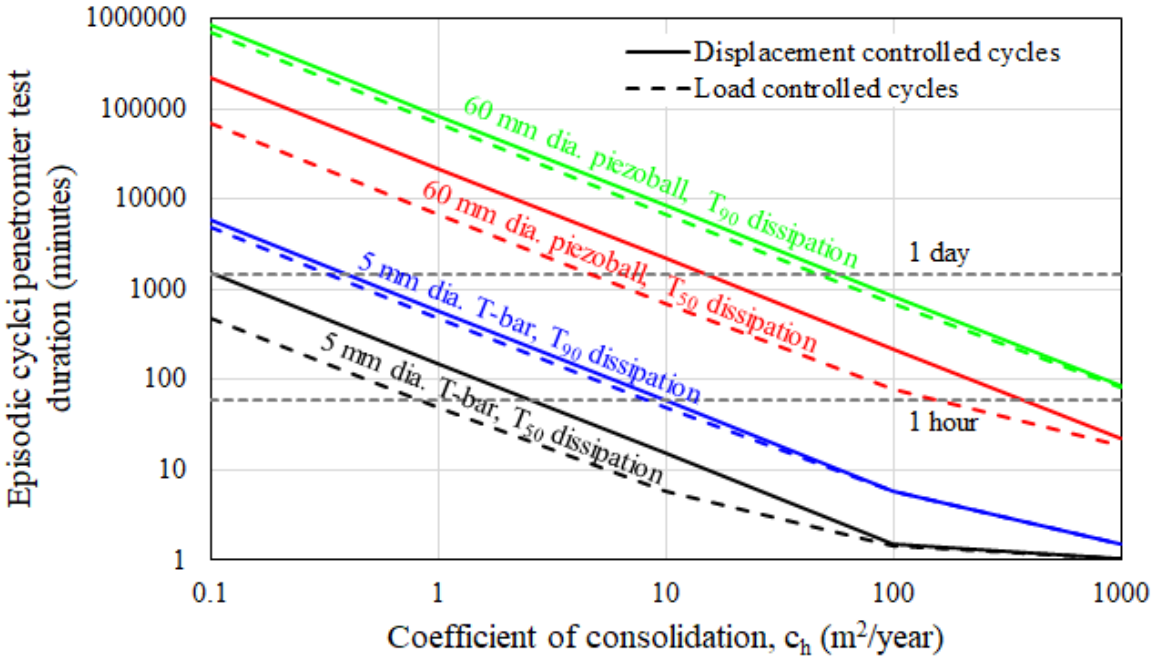

Figure 18. Estimated durations of episodic cyclic penetrometer tests assuming a rigidity index, $I_r = 100$.

5. Conclusions

The data considered in this paper highlight the benefits of full-flow penetrometers for profiling soft soils, allowing for measurements of intact and remoulded soil strength and the consolidation coefficient in a single test. Excess pore pressure dissipation around a piezoball is quicker than around a piezocone, despite the larger diameter of the piezoball, in both numerical simulations and field testing. The consolidation coefficient may be calculated from the dissipation response, and the piezoball is subject to less uncertainty associated with the assumed soil rigidity index. The data also indicate the need to assess whether the penetration response is undrained, as this will affect interpretations of soil strength from the net penetration resistance, and may also affect the back-figured consolidation coefficient from the dissipation phase of the test, particularly if the penetration response is partially drained.

New test protocols are introduced that quantify the rate and magnitude of strength changes due to the combined effect of cyclic remoulding or loading and reconsolidation. Such tests are likely to be better suited to box-cores or tube samples recovered from the seabed as they can be conducted off the critical path of vessel operations. They provide data that could potentially be used to support assessment of the long-term operative strength of foundations, piles and anchors that are subjected to loading events that are accompanied by drainage and consolidation. This may in turn unlock design benefits of increased soil strength that are currently overlooked.

Further work is required to establish interpretation methodologies that allow these results to be interpreted into parameters that can then be used in the design assessments. However, groundwork has already been laid in this direction, via parallel work into the changing strength of soil beneath foundations and pipelines using a simplified critical state framework (e.g. White & Hodder 2010; White et al. 2015; Zhou et al. 2019, 2020a, 2020b). Meanwhile, existing literature has addressed the same process at soil element level (e.g. Yasuhara 1994).

6. References

[1] Andersen, K.H., Murff, J.D., Randolph, M.F., Clukey, E.C., Erbrich, C.T., Jostad, H.P., Hansen, B., Aubeny, C.P., Sharma, P. & Supachawarote, C. (2005). Suction anchors for deepwater applications. Proceedings of the 1st International Symposium on Frontiers in Offshore Geotechnics, Perth, Australia, 3–30.

[2] Borel, D., Puech, A., Dendani, H. & Colliat, J.L. (2005). Deepwater geotechnical site investigation practice in the Gulf of Guinea. Proceedings of the 1st International Symposium on Frontiers in Offshore Geotechnics, Perth, Australia, 921–926.

[3] Borel, D., Puech, A. & Po, S. (2010). A site investigation strategy to obtain fast-track shear strength design parameters in deep water soils. Proceedings of the 2nd International Symposium on Frontiers in Offshore Geotechnics, Perth, Australia, 253-258.

[4] Boylan, N., Long, M., Ward, D., Barwise, A. & Georgious, B. (2007). Full-flow penetrometer testing in Bothkennar clay. Proceedings of the 6th International Offshore Site Investigation and Geotechnics Conference: Confronting New Challenges and Sharing Knowledge, Society for Underwater Technology, London, UK, 177–186.

[5] Boylan, N., Randolph, M. F. & Low, H. E. (2010). Enhancement of the ball penetrometer test with pore pressure measurements. Proceedings of the 2nd International Symposium on Frontiers in Offshore Geotechnics, Perth, Australia, 259–264.

[6] Chai, J., Sheng, D., Carter, J. P. & Zhu, H. (2012). Coefficient of consolidation from non-standard piezocone dissipation curves. Computers and Geotechnics, 41, 13–22.

[7] Cocjin M., Gourvenec S.M., White D.J. & Randolph M.F. (2017). Theoretical framework for predicting the response of tolerably mobile subsea installations. Géotechnique, 67(7), 608–620.

[8] Colreavy, C., O'Loughlin, C.D. & Randolph, M.F. (2016a). Estimating consolidation parameters from field piezoball tests. Géotechnique, 66(4), 333–343.

[9] Colreavy, C., O'Loughlin, C.D. & Randolph, M.F. (2016b). Experience with a dual pore pressure element piezoball. International Journal of Physical Modelling in Geotechnics, 16(3), 101–118.

[10] DeJong, J.T., Yafrate, N.J. & Randolph, M.F. (2008). Use of a Full Flow Ball Penetrometer with Pore Pressure Measurements in Soft Clay. Proceedings of ISC-3: 3rd International Conference on Site Characterization, Taipei, 269–1275.
[11] Einav, I. & Randolph, M.F. (2005). Combining upper bound and strain path methods for evaluating penetration resistance. International Journal for Numerical Methods in Engineering, 63(14), 1991-2016.
[12] Erbich (2005). Australian frontiers – spudcans on the edge. Proceedings of the 1st International Symposium on Frontiers in Offshore Geotechnics, Perth, Australia, 29–74.
[13] Hodder, M. S., White, D. J. & Cassidy, M. J. (2009). Effect of remolding and reconsolidates on the touchdown stiffness of a steel catenary riser: Observations from centrifuge modelling. Proceedings of the Offshore Technology Conference, Houston, USA, OTC 19871-PP.
[14] House, A., Oliveiria, J.R.M.S. & Randolph, M.F. (2001). Evaluating the coefficient of consolidation using penetration tests. International Journal of Physical Modelling in Geotechnics, 1(3), 17–26.
[15] Kelleher, P., Low, H. E., Jones, C., Lunne, T., Strandvik, S. & Tjelta, T. I. (2010). Strength measurement in very soft upper seabed sediments. Proceedings of the 2nd International Symposium on Frontiers in Offshore Geotechnics, Perth, Australia, 283–288.
[16] Low, H.E., Randolph, M.F. & Kelleher, P. (2007) Estimation of in-situ coefficient of consolidation from dissipation tests with different penetrometers. Proceedings of the International Conference on Offshore Site Investigation and Geotechnics, Society for Underwater Technology, London, 547–556.
[17] Lunne, T., Robertson, P. K. & Powell, J. J. M. (1997). Cone Penetration Testing in Geotechnical Practice. Blackie Academic and Professional, London.
[18] Mahmoodzadeh, H., Wang, D. & Randolph, M.F. (2015). Interpretation of piezoball dissipation testing in clay. Géotechnique, 65(10), 831–842.
[19] O'Loughlin, C.D., Zhou, Z., Stanier, S.A. & White, D.J. (2020) Load-controlled cyclic T-bar tests: a new method to assess effects of cyclic loading and consolidation. Géotechnique Letters, 10(1), 7–15.
[20] Peuchen, J., Adrichem, J. & Hefer, P. A. (2005). Practice notes on push-in penetrometers for offshore geotechnical investigation, Proceedings of the 1st International Symposium on Frontiers in Offshore Geotechnics, Perth, Australia, 973–979.
[21] Randolph, M. F. & Hope, S. (2004). Effect of cone velocity on cone resistance and excess pore pressures. Proceedings of the International Symposium on Engineering Practice and Performance of Soft Deposits, Osaka, Japan, 147–152.
[22] Randolph MF, Low HE & Zhou H (2007) In situ testing for design of pipeline and anchoring systems. Proceedings of the 6th International Conference on Offshore Site Investigation and Geotechnics: Confronting New Challenges and Sharing Knowledge, Society of Underwater Technology, London, UK, 251–262.
[23] Stewart, D.P., and Randolph, M.F. (1991) A new site investigation tool for the centrifuge. Proceedings of the International Conference on Centrifuge Modelling, Centrifuge '91, Boulder, USA, 531–538.
[24] Sully, J. P., Robertson, P. K., Campanella, R. G. & Woeller, D. J. (1999). An approach to evaluation of field CPTU dissipation data in overconsolidated fine-grained soils. Canadian Geotechnical Journal, 36(2), 369–381.
[25] Suzuki, Y. (2015). Investigation and interpretation of cone penetration rate effects. Ph.D. thesis, University of Western Australia, Crawley, Australia.
[26] Teh, C. I. & Houlsby, G. T. (1991). An analytical study of the cone penetration test in clay. Géotechnique, 41(1), 17–34.
[27] White, D.J. & Hodder, M.S. (2010). A simple model for the effect on soil strength of remoulding and reconsolidation. Canadian Geotechnical Journal, 47(7), 821–826.
[28] White D.J., Westgate Z., Ballard J-C, de Brier C. & Bransby M.F. (2015). Best practice geotechnical characterization and pipe-soil interaction analysis for HPHT flowline design. Proceedings of the Offshore Technology Conference, Houston, USA, OTC26026-MS.
[29] White, D.J., Clukey, E.C., Randolph, M.F., Boylan, N.P., Bransby, M.F., Zakeri, A., Hill, A.J. & Jaeck, C. (2017). The state of knowledge of pipe-soil interaction for on-bottom pipeline design. Proceedings of the Offshore Technology Conference, Houston, USA, OTC 27623.
[30] Wong, P., Gaudin, C., Randolph, M.F., Cassidy, M J. & Tian, Y. (2012). Performance of suction embedded plate anchors in permanent mooring applications. Proceedings of the 22nd ISOPE Conference, Rhodes, Greece, 2, 640–645.
[31] Yasuhara K. (1994). Post-cyclic undrained strength for cohesive soils. ASCE Journal of Geotechnical. Engineering, 120(11), 1961–1979.
[32] Zhou, Z. White, D.J. & O'Loughlin, C.D. (2019). An effective stress framework for estimating penetration resistance accounting for changes in soil strength from maintained load, remoulding and reconsolidation. Géotechnique, 69(1), 57–71.
[33] Zhou, Z., O'Loughlin, C.D. & White, D.J. (2020a). An effective stress analysis for predicting the evolution of SCR-seabed stiffness, accounting for consolidation. Géotechnique, in press, doi: 10.1680/jgeot.18.P.313.
[34] Zhou, Z., O'Loughlin, C.D., White, D.J. & Stanier, S.A. (2020b). Improvements in plate anchor capacity due to cyclic and maintained loads combined with consolidation. Géotechnique, in press, doi: 10.1680/jgeot.19.ti.028.